BJ www.biochemj.org

BJ Cell

Biochem. J. (2011) **437**, 389–397 (Printed in Great Britain) doi:10.1042/BJ20110706

Intrinsic membrane association of the cytoplasmic tail of influenza virus M2 protein and lateral membrane sorting regulated by cholesterol binding and palmitoylation

Bastian THAA*, Ilya LEVENTAL†, Andreas HERRMANN‡ and Michael VEIT*[1]

*Faculty of Veterinary Medicine, Institute of Immunology and Molecular Biology, Free University Berlin, Philippstrasse 13, 10115 Berlin, Germany, †Max Planck Institute of Molecular Cell Biology and Genetics, Pfotenhauerstrasse 108, 01307 Dresden, Germany, and ‡Institute of Biology, Molecular Biophysics, Humboldt University, Invalidenstrasse 42, 10115 Berlin, Germany

The influenza virus transmembrane protein M2 is a proton channel, but also plays a role in the scission of nascent virus particles from the plasma membrane. An amphiphilic helix in the CT (cytoplasmic tail) of M2 is supposed to insert into the lipid bilayer, thereby inducing curvature. Palmitoylation of the helix and binding to cholesterol via putative CRAC (cholesterol recognition/interaction amino acid consensus) motifs are believed to target M2 to the edge of rafts, the viral-budding site. In the present study, we tested pre-conditions of this model, i.e. that the CT interacts with membranes, and that acylation and cholesterol binding affect targeting of M2. M2-CT, purified as a glutathione transferase fusion protein, associated with [^{3}H]photocholesterol and with liposomes. Mutation of tyrosine residues in the CRAC motifs prevented [^{3}H]photocholesterol labelling and reduced liposome binding. M2-CT fused to the yellow fluorescent protein localized to the Golgi in transfected cells; membrane targeting was dependent on CRAC and (to a lesser extent) on palmitoylation. Preparation of giant plasma membrane vesicles from cells expressing full-length M2–GFP (green fluorescent protein) showed that the protein is partly present in the raft domain. Raft targeting required palmitoylation, but not the CRAC motifs. Thus palmitoylation and cholesterol binding differentially affect the intrinsic membrane binding of the amphiphilic helix.

Key words: cholesterol binding, cholesterol recognition/interaction amino acid consensus (CRAC) motif, giant plasma membrane vesicle, M2, membrane raft, palmitoylation.

INTRODUCTION

The assembly and budding of influenza virus particles is organized in membrane raft domains in the apical plasma membrane of infected cells [1,2]. Membrane rafts are dynamic lateral plasma membrane nanodomains enriched in cholesterol and sphingolipids; they can be coalesced into larger more stable platforms by protein–protein and protein–lipid interactions to specifically include certain proteins and exclude others [3]. Raft-targeting of the transmembrane glycoproteins of influenza virus, HA (haemagglutinin) and NA (neuraminidase), defines the site of assembly and budding, the 'viral budozone', a stabilized and large raft domain [4,5]. However, the third viral transmembrane protein, the proton channel M2, is assumed to be excluded from membrane raft domains. It does not associate with detergent-resistant membranes, the controversial biochemical correlate of membrane rafts [6], and does not cluster with small unstable rafts when expressed in the absence of other viral proteins [7]. Accordingly, M2 is largely excluded from mature virus particles [8].

However, numerous reports point to a role for M2 in assembly, budding and scission of nascent virus particles, independent of its proton channel activity [9–13]. Thus at least some M2 molecules have to associate with the viral budozone in the process of virus assembly. In line with this proposal, M2 was found to localize to the base of budding virus particles [14] and to cluster with HA, even in the absence of other viral proteins [7].

M2 is a homotetramer of 97 amino acids/monomer with the first 24 residues orientated towards the outside (ectodomain), the next 19 residues forming a TMD (transmembrane domain), and the remaining 54 residues (amino acids 44–97) constituting the CT (cytoplasmic tail) [8]. The CT contains a binding site (amino acid residues 71–73) for the viral matrix protein M1, the main organizer of virus assembly [9]. The interaction with M2 is probably required for transport of M1 from internal membranes, where it accumulates in the absence of other virus proteins, to the viral budozone [15,16].

The TMD of M2 is followed by a stretch of basic and hydrophobic amino acids (residues 51–60) that is thought to form an amphiphilic helix. Two partly conflicting NMR structures of the TMD region, plus adjacent helix, have been published [17,18]. The structure of detergent-solubilized M2 revealed that the amphiphilic helices form a tetrameric bundle that would extend into the cytoplasm [17]. In contrast, when the structure of membrane-embedded M2 was determined, the part adjacent to the TMD (residues 47–50) formed a tight loop and the amphiphilic helices were located in the interfacial region of the lipid bilayer [18], as shown in Figure 1(a). The latter structure is also consistent with electron paramagnetic resonance measurements [19], which indicate that the most hydrophobic residues of the helix are

Abbreviations used: CHO, Chinese-hamster ovary; CRAC, cholesterol recognition/interaction amino acid consensus; CT, cytoplasmic tail; DMEM, Dulbecco's modified Eagle's medium; ER, endoplasmic reticulum; FBS, fetal bovine serum; GFP, green fluorescent protein; GPMV, giant plasma membrane vesicle; GST, glutathione transferase; GUV, giant unilamellar vesicle; HA, haemagglutinin; Ld, liquid-disordered; Lo, liquid-ordered; LUV, large unilamellar vesicle; M2-CT, cytoplasmic tail of M2; MβCD, methyl-β-cyclodextrin; NEM, *N*-ethylmaleimide; ORF, open reading frame; PC, phosphatidylcholine; RBL, rat basophilic leukaemia; RhPE, rhodamine-phosphatidylethanolamine; TMD, transmembrane domain; wt, wild-type; YFP, yellow fluorescent protein.

[1] To whom correspondence should be addressed (email mveit@zedat.fu-berlin).

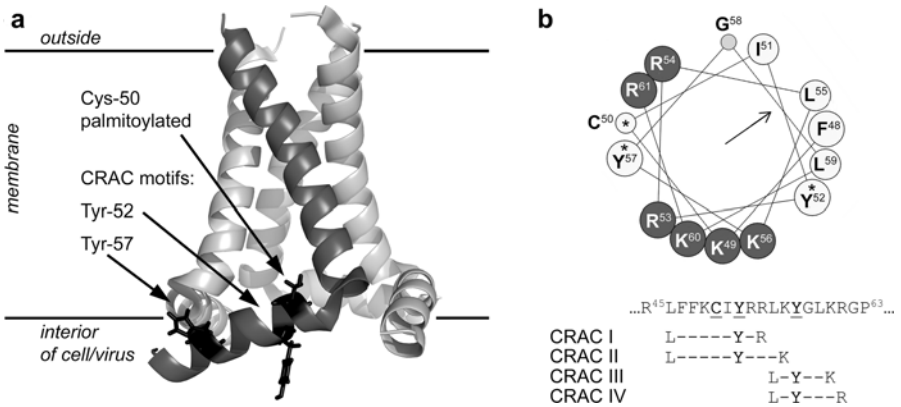

Figure 1 Structure of M2 and its amphiphilic helix

(**a**) Structure of the M2 tetramer (residues 22–62) according to solid-state NMR spectroscopy [18]. One monomer is highlighted in dark grey. Potential raft-targeting features in the membrane-parallel amphiphilic helix (residues 48–61) are shown as sticks: the palmitoylation site Cys^{50} (a serine residue is present in the M2 analysed by NMR); and Tyr^{52} and Tyr^{57} (a histidine residue is present at position 57 in the M2 analysed by NMR) as part of the CRAC motifs. The Figure was generated with PyMOL (http://www.pymol.org) from PDB code 2L0J. (**b**) Helical wheel plot (axial view) of the amphiphilic helix formed by amino acids 48–61 of M2 from Influenza A/Duck/Ukraine/63/1 (H3N8), generated with HeliQuest (http://heliquest.ipmc.cnrs.fr/). Hydrophobic residues are represented in light grey, and hydrophilic residues are represented in dark grey. The arrow indicates the direction of the calculated hydrophobic moment [39]. However, in the Figure the helix is orientated with respect to the plane of the membrane according to the NMR structure [18]. The residues that were replaced in the present study (Cys^{50}, Tyr^{52} and Tyr^{57}) are labelled with asterisks. The sequence of amino acids 45–63 in the M2 analysed in the present study and the position of the four CRAC motifs are indicated in the bottom part of the Figure.

membrane-embedded, whereas the basic residues are water-exposed.

Neither of these NMR structures comprise the two lipid modifications of the amphiphilic helix, S-acylation ('palmitoylation') at Cys^{50} [20,21] and binding of cholesterol. Full-length M2 has been described to co-purify with cholesterol in stoichiometric amounts [22]. It was proposed that cholesterol binding is mediated by a CRAC (cholesterol recognition/interaction amino acid consensus) motif (L/V-$X_{1–5}$-Y-$X_{1–5}$-R/K) [23], which is present up to four times in the amphiphilic helix region of the CT of M2, dependent on the virus strain [22,24] (Figure 1b). However, it has not been determined experimentally whether cholesterol binds to the CRAC motifs alone and/or whether the transmembrane region is required.

Since palmitoylation is a typical raft-targeting feature of proteins [25] and cholesterol is the decisive lipid component of membrane rafts [26], it was proposed that M2 might accumulate at the edge of rafts. The fatty acid moiety and cholesterol might associate with the raft domain, but the relatively short transmembrane region of M2 prevents complete immersion of the protein in the more ordered, hence thicker, raft domains [22]. Moreover, amphiphilic helices are typical membrane remodelling structures as they can intrude like a wedge into the membrane and thereby induce curvature [27,28]. Thus the amphiphilic helix of M2 could be involved in curvature formation during budding and ultimately in scission of the nascent virus particle from the membrane [22]. Recently it was shown that a peptide encompassing the amphiphilic helix of M2 can specifically lead to the formation of vesicles in model membrane systems, providing evidence for a role of this region in the scission process [29].

However, proof of this concept in the context of virus infection produced ambiguous results. Neither the CRAC motifs nor acylation are absolutely essential for the production of virus particles: there are virus strains in which the acylation site or intact CRAC motifs are lacking, and recombinant viruses in which Cys^{50} [30,31] or parts of the CRAC motifs [32] were replaced grew similarly well as the corresponding wt (wild-type) virus, at least in cell culture. Five hydrophobic residues in the hydrophobic part of the amphiphilic helix of M2-CT had to be mutated to observe an effect on virus shape, virus titre and vesicularization capacity; mutation of less residues had no effect [14,29]. Thus the contribution of acylation and the CRAC motifs on virus reproduction is probably subtle and possibly compensated for by other viral factors.

In the present study, we have analysed whether the purified CT of M2 binds cholesterol, and if this binding is affected by mutations in the CRAC motifs. The proposed role for the amphiphilic helix in membrane remodelling and scission depends on efficient membrane association. Hence we sought to determine whether the CT of M2 has an intrinsic propensity to associate with membranes, both *in vitro* and in transfected cells, and to analyse to what extent this is influenced by palmitoylation and the CRAC motifs. Furthermore, we analysed whether authentic M2 associates with large raft domains produced in a novel model membrane system, and how palmitoylation and/or CRAC motifs could modulate intrinsic lateral sorting of M2.

EXPERIMENTAL

Plasmids

The ORFs (open reading frames) of M2 from Influenza A/Duck/Ukraine/1/63 (H3N8), wt sequence and encoding the replacement of Tyr^{52} and Tyr^{57} by serine residues (Y52S,Y57S) were synthesized *in vitro* (ATG Biosynthetics). From these, the sequence encoding M2-CT, corresponding to amino acids 44–97, was amplified by PCR and subcloned into pGEX-6P-1 (GE Healthcare) using the EcoRI and NotI restriction sites, or into pEYFP-N1 (Clontech) using SacII and AgeI, for the expression of the GST (glutathione transferase)-fusion protein GST–M2-CT in *Escherichia coli* and M2-CT fused to YFP (yellow fluorescent protein) in CHO (Chinese-hamster ovary) cells respectively. M2–GFP (green fluorescent protein) expression plasmids were generated by subcloning the full-length ORF encoding M2 into pEGFP-C1 using AgeI and NheI. The nucleotides encoding Cys^{50} (TGT) were replaced by a serine codon (TCA) in M2-wt and the M2-Y52S,Y57S sequences by site-directed mutagenesis using overlap-extension PCR [33],

yielding M2-C50S and M2-C50S,Y52S,Y57S respectively. All constructs were checked for correctness by sequencing (GATC).

Expression and purification of GST–M2-CT

Recombinant proteins (GST–M2-CT wt, GST–M2-CT Y52S, Y57S and unmodified GST) were produced in *E. coli* BL21(DE3) cells transformed with the respective expression plasmids. After growing the bacteria in YT (yeast-tryptone) medium (Invitrogen) containing 100 μg/ml ampicillin at 37 °C to a D_{600} of approximately 0.5, expression was induced by the addition of 100 μM IPTG (isopropyl β-D-thiogalactopyranoside), growth was continued at 21 °C for 6 h, cells were harvested by centrifugation (10000 ***g*** for 10 min at 4 °C), and pellets were stored at − 20 °C. Cells were lysed by sonication (Misonix XL-2000, Misonix; six 10 s pulses of 15 W) in PBS supplemented with 1 mM PMSF, 1 mM DTT (dithiothreitol), DNase I (Roche) and protease inhibitor cocktail (Serva). After clearing by ultracentrifugation (Beckman Ti-45 rotor; 23000 rev./min for 45 min at 4 °C), the lysate was loaded on to a GSTrap affinity-chromatography column (5 ml volume, GE Healthcare). After washing with PBS, the GST-containing protein was eluted with 50 mM Tris/HCl (pH 7.5) containing 10 mM GSH (Sigma–Aldrich) and concentrated using an Amicon ultrafilter (molecular mass cut-off of 10 kDa, Millipore). Purity of the protein preparation was checked by SDS/PAGE, and the protein concentration was determined spectrophotometrically (NanoDrop 1000, Peqlab). Protease inhibitors (mix G, Serva) were present throughout the purification.

[^{3}H]Photocholesterol cross-linking

[^{3}H]Photocholesterol was synthesized and complexed with MβCD (methyl-β-cyclodextrin) as described previously [34]. For labelling, purified recombinant protein (20 μg) in 50 mM Tris/HCl (pH 7.5) was incubated with 10 μCi of MβCD-complexed [^{3}H]photocholesterol for 30 min at 4 °C, followed by illumination with UV light (wavelength 320–365 nm, power 8 W) for 20 min. The samples were then separated by SDS/PAGE and fluorography as described below.

Liposome-binding assay

LUVs (large unilamellar vesicles) were produced by extrusion. The required lipids [PC (phosphatidylcholine) from egg and cholesterol (Sigma–Aldrich)] solubilized in chloroform/methanol (3:1, v/v) were mixed in a glass tube, the solvent was evaporated under nitrogen flow, the lipid film was dried under vacuum and subsequently resolubilized (lipid concentration 1 mg/ml) in 50 mM Tris/HCl (pH 7.5), for 1 h at 22 °C, followed by ultrasonication for 10 min and 15 extrusion steps through a polycarbonate filter (pore size of 100 nm) using a mini-extruder (Avanti Polar Lipids), yielding LUVs with a mean diameter of 100 nm. To detect protein binding, the LUVs (1.5 mM) were incubated with purified recombinant protein (6 μM) in a reaction volume of 80 μl for 30 min at 22 °C, then mixed with 240 μl of 105 % (w/v) Nycodenz (Sigma–Aldrich) in 50 mM Tris/HCl (pH 7.5), and overlayered with 720 μl of 58 % (w/v) Nycodenz and 240 μl of 8 % Nycodenz and subjected to ultracentrifugation (Beckman TLA-100.2 rotor, 60000 rev./min for 4 h at 4 °C). Following this, the gradient was divided into four fractions of equal size from top to bottom, subjected to protein precipitation with 10 % (w/v) trichloroacetic acid and analysed by SDS/PAGE and Coomassie Brilliant Blue G-250 staining. Densitometric analysis of bands was accomplished using Bio one-dimensional software (Vilber-Lourmat) after imaging of the gel with a Fusion SL camera system (PeqLab).

Cells and transfections

CHO-K1 cells (A.T.C.C. CCL-61) were cultured in DMEM (Dulbecco's modified Eagle's medium)+10 % FBS (fetal bovine serum) at 37 °C in 5 % CO_2, using standard techniques; RBL (rat basophilic leukaemia) cells (A.T.C.C. CRL-2256) were grown in 30 % DMEM+60 % RPMI 1640 + 10 % FBS supplemented with 2 mM L-glutamine, 100 units/ml penicillin and 100 μg/ml streptomycin.

Transient transfections of CHO cells were performed in 35 mm dishes (Greiner Bio-One) using Lipofectamine™ 2000 (Invitrogen) or TurboFect (Fermentas) in OptiMEM medium (Invitrogen) according to the manufacturer's instructions. RBL cells were transfected using an Amaxa nucleofector (Lonza), program T-30.

Immunofluorescence and confocal microscopy

To assess subcellular localization, the protein in question was expressed as a YFP-fusion protein. The cells, grown on coverslips, were fixed 24 h after transfection with 3 % (w/v) paraformaldehyde in PBS for 10 min, permeabilized with 0.5 % Triton X-100 in PBS for 3 min, blocked (3 % BSA in PBS for 1 h), incubated with primary antibody in blocking solution for 45 min [marker for the ER (endoplasmic reticulum), rabbit anti-calreticulin (Calbiochem/Merck); marker for the Golgi apparatus, mouse anti-membrin (Abcam), at the recommended dilutions], treated with Alexa Fluor® 568-labelled secondary antibody for 45 min (anti-rabbit and anti-mouse respectively, Molecular Probes/Invitrogen, at a 1:1000 dilution), and mounted on microscope slides. Washing with PBS (three times, each for 2 min) was performed between each step.

Confocal laser-scanning microscopy was carried out with an Olympus FluoView 1000 microscope using an UPLSAPO ×60 oil-immersion objective (numeric aperture, 1.35). YFP fluorescence was excited with a 515 nm argon laser and recorded at 535–575 nm, excitation of Alexa Fluor® 568 fluorescence was performed using the 559 nm line of a HeNe laser, and the emission was detected between 580 and 664 nm. Images were processed and assessed for co-localization using ImageJ and Adobe Photoshop 7.0.

Metabolic labelling with [^{3}H]palmitate and immunoprecipitation

To biochemically test for S-acylation of proteins, metabolic labelling was performed as described previously [33]. Cells were washed with PBS 24 h after transfection and then incubated with 250 μCi of [^{3}H]palmitate (Hartmann Analytic, administered in 10 μl of ethanol to 500 μl of DMEM without serum) for 4 h at 37 °C and 5 % CO_2. Following this, cells were washed with PBS, lysed with 600 μl of RIPA buffer [50 mM Tris/HCl (pH 7.4), 150 mM NaCl, 10 mM EDTA, 10 mM iodoacetamide, 0.1 % SDS, 1 % (w/v) Triton X-100, 1 % (w/v) sodium deoxycholate and Serva protease inhibitor mix G] on ice for 15 min and centrifuged (20000 ***g*** for 20 min at 4 °C). The supernatant was treated with 1.6 μg of anti-GFP antibody (Molecular Probes/Invitrogen), incubated for 16 h at 4 °C under shaking (600 rev./min), and mixed with 40 μl of a 1:1 slurry of Protein A–Sepharose (Sigma–Aldrich) in RIPA buffer to precipitate antibody–protein complexes. After 2.5 h of shaking (600 rev./min) at 4 °C, the samples were centrifuged (800 ***g*** for 3 min at 25 °C) and washed four times with RIPA buffer, followed

by treatment of the resulting pellets with non-reducing SDS/PAGE loading buffer. After separation by SDS/PAGE, gels were treated with fixing solution [10 % (v/v) acetic acid and 10 % (v/v) ethanol in water, for 16 h at 22 °C], water (twice for 15 min each) and 1 M salicylate in water (30 min), and then dried with a gel dryer (UniEquip). A Kodak BioMax XAR film (Sigma–Aldrich) was put on the dried gel, exposed for up to 3 months and then developed using Kodak GBX developing/fixing solutions (Sigma–Aldrich).

As a control for expression and immunoprecipitation, labelling with [^{35}S]methionine/cysteine was performed in parallel. At 24 h after transfection, the cell culture medium was replaced with DMEM not containing methionine and cysteine (PAN). After 2 h of incubation at 37 °C and 5 % CO_2, 50 μCi of Tran35S-Label (MP Biomedicals) was added and incubation was continued for 4 h, followed by cell lysis and immunoprecipitation as described above.

GPMVs (giant plasma membrane vesicles)

GPMVs were generated using a method described by Levental et al. [35]. Briefly, RBL cells (grown in 25 cm^2 flasks) were washed with GPMV buffer [10 mM Hepes (pH 7.4), 150 mM NaCl and 2 mM $CaCl_2$] 24 h after transfection with M2–GFP and subsequently incubated with GPMV buffer plus 2 mM NEM (*N*-ethylmaleimide) at 37 °C for 1 h with gentle shaking (60 rev./min). The GPMV-rich supernatant was then transferred to a microscope chamber for temperature-controlled imaging. Phase separation into raft-like and non-raft phases was induced by cooling the vesicles below ~7 °C. To label the non-raft phase, RhPE (rhodamine-phosphatidylethanolamine, 3.75 μg/ml) was applied to the cells 7 min before GPMV production. GPMVs were analysed by epifluorescence microscopy as described previously [35]. The raft-partitioning coefficient C_R was calculated by dividing the background-subtracted peak intensity of M2–GFP in the raft phase by that of the non-raft phase, as described previously [35].

RESULTS AND DISCUSSION

CRAC motifs in the amphiphilic helix of M2 bind cholesterol

Figure 1(b) shows a helical wheel plot (http://heliquest.ipmc.cnrs.fr/) of the amphiphilic helix formed by amino acids 48–61 of M2. One side of the helix contains a cluster of basic amino acids, which, as observed in the NMR structure of M2 [18], point outward such that they could interact with negatively charged phospholipids abundant at the inner leaflet of the plasma membrane. The other side of the helix shows large hydrophobic amino acids, such as phenylalanine, isoleucine and leucine, which in principle could interact with the hydrophobic interior of lipid bilayers. Both sides of the helix are bordered by tyrosine residues, which can associate with the interfacial region of a bilayer. The algorithm used to create the helical wheel plot also calculates a mean hydrophobicity of 0.318, a hydrophobic moment of 0.51 and a net charge of +6 for the M2 helix. A comparison of these three biophysical parameters with those of 21 different lipid-binding amphiphilic helices reveals that the M2 helix has the highest similarity with Arf1 and endophilin A1, components of the vesicular transport machinery known to induce membrane curvature, and with the antibacterial peptide magainin 2, which forms pores in membranes [27].

A unique property of the amphiphilic helix of M2 is the presence of two specific lipid-association features: palmitoylation and putative cholesterol-binding CRAC motifs (L/V-$X_{1–5}$-Y-$X_{1–5}$-R/K). The modification of Cys^{50} with palmitate, another potential membrane-anchoring moiety [36], is peculiar since there is only one other amphiphilic helix known to be acylated (in Arf1, which contains myristate at the N-terminal glycine residue [27]). To our knowledge, cholesterol binding has not been described for any amphiphilic helix.

There are up to four possible CRAC motifs in M2, depending on the virus strain; in some rare cases, such as for the filamentous strain Udorn, the M2 sequence does not fit the consensus [22,24]. In order to disrupt all four possible CRAC motifs in the M2 of Influenza virus A/Duck/Ukraine/63/1 (H3N8), we replaced the two tyrosine residues (Tyr^{52} and Tyr^{57}) by serine residues, yielding the mutant M2-Y52S,Y57S (Figure 1 shows the location of the tyrosine residues within the amphiphilic helix). The same strategy impeded cholesterol association in other CRAC motif-containing proteins [37,38]. Importantly, performing the helical wheel plot with the mutated M2 sequence revealed that the mean hydrophobicity was reduced to 0.265, but the overall organization of the helix, as well as the hydrophobic moment (0.55), a measure of the amphiphilicity of a helix [39], remained virtually unchanged.

First, we checked whether M2-CT (residues 44–97) binds cholesterol, and whether the tyrosine residues of the CRAC motifs are directly involved. To this end, we used [^{3}H]photocholesterol, which can be covalently cross-linked to various cellular cholesterol-binding proteins upon UV illumination [34,40–42]. We expressed M2-CT fused to GST (GST–M2-CT), as wt or the Y52S,Y57S mutant, in *E. coli*, purified the proteins by affinity chromatography, and incubated with the cholesterol probe [34], which was administered in a complex with MβCD owing to the poor solubility of cholesterol in water and to avoid artefacts from the potential formation of [^{3}H]photocholesterol micelles. Illumination with UV light, SDS/PAGE and fluorography revealed that [^{3}H]photocholesterol cross-linking occurred for GST–M2-CT wt, but not for the Y52S,Y57S mutant (Figure 2, black arrow). The cross-linking was specific for M2-CT since free GST, which was also present in the GST–M2-CT preparations, was not labelled by [^{3}H]photocholesterol (Figure 2, grey arrow). The identity of two other ^{3}H signals (marked with asterisks) is unclear as they cannot be assigned to any of the protein bands detectable by Coomassie Blue staining of the gel. Not only does this finding corroborate that M2-CT binds to cholesterol, but it furthermore provides the first experimental evidence that Tyr^{52} and/or Tyr^{57}, the central amino acids in the CRAC motifs, are critical for this interaction. The limited availability of the material did not allow further analysis of the binding site. However, note that neither the TMD nor palmitoylation at Cys^{50} were needed for cross-linking of GST–M2-CT to the cholesterol probe because proteins expressed in *E. coli* are generally not acylated [36].

The amphiphilic helix binds M2-CT to LUVs

Membrane binding, especially via the amphiphilic helix, is a prerequisite for the suggested role of M2-CT in membrane remodelling and virus particle scission. The authentic M2 protein is stably membrane-anchored by its transmembrane region, and thus possible membrane interactions of its CT cannot be analysed in that context. Therefore we sought to determine whether the CT alone has the capacity to interact with membranes. We incubated purified GST–M2-CT (wt or Y52S,Y57S mutant) with LUVs, either made from PC (from egg), resembling the major constituent of cell membranes, or from PC plus cholesterol (molar ratio 3:2). Samples were then centrifuged in a density gradient, which was subsequently divided into four fractions. The amount of protein in each fraction was evaluated by SDS/PAGE and Coomassie Blue staining. In the absence of LUVs, proteins

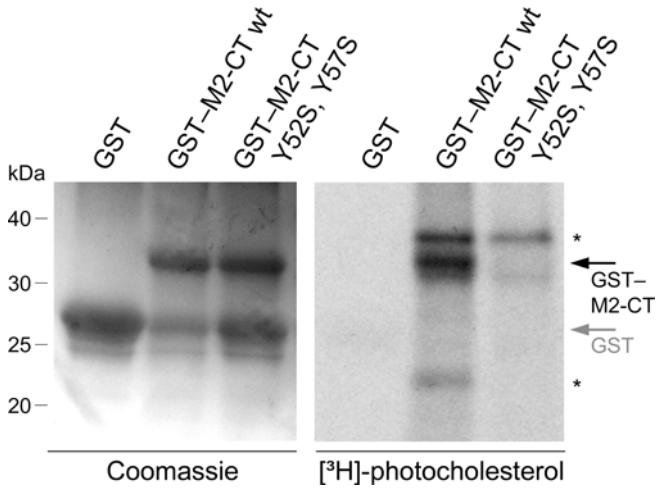

Figure 2 Cross-linking of GST–M2-CT to [^{3}H]photocholesterol

Purified GST, GST–M2-CT wt or GST–M2-CT-Y52S,Y57S were incubated with MβCD-complexed [^{3}H]photocholesterol, UV cross-linked, separated by SDS/PAGE and subjected to Coomassie Blue staining (left-hand panel) and fluorography (right-hand panel). Black arrow, GST–M2-CT; grey arrow, GST; asterisks, unassigned bands. Molecular mass markers in kDa are indicated on the left-hand side.

remained at the bottom of the gradient, in fractions c and d, which were therefore defined as unbound protein (Figure 3a, lowermost panels). In the presence of LUVs, which float to the top of the density gradient, proteins are partly or predominantly present in fractions a and b (Figure 3a, upper panels).

Densitometric quantification of four independent experiments (Figure 3b) revealed that GST alone has a low intrinsic membrane interaction capacity, approximately 20 % of total protein was present in the top fractions of the gradient. In contrast, almost 80 % of GST–M2-CT wt was detectable in fractions a and b (compare the black and white columns), indicating that M2-CT has a strong propensity to associate with membranes. The Y52S,Y57S mutant bound less strongly (40 % in the top fractions) to LUVs than the corresponding wt protein, but was still significantly stronger than free GST (grey columns). This might indicate that cholesterol binding via the CRAC motifs enhances membrane binding of M2-CT. However, omission of cholesterol in the LUVs did not change the percentage of membrane-bound molecules, neither of M2-CT wt nor of the Y52S,Y57S mutant.

In summary, M2-CT has the capacity to interact with artificial membranes. This interaction is likely to be mediated by the amphiphilic helix, given that the remaining part of the CT is highly hydrophilic and contains numerous negatively charged amino acids that are unlikely to interact with membranes. The results indicate that the tyrosine residues in the amphiphilic helix directly associate with the interfacial region of the bilayer, but cholesterol is not required for membrane association of M2-CT in this assay.

The amphiphilic helix binds M2-CT to cellular membranes

In the next set of experiments we analysed the membrane-interaction capacity of M2-CT in eukaryotic CHO cells. M2-CT was fused to the N-terminus of YFP, yielding M2-CT–YFP. YFP, when expressed alone, has no membrane-targeting features and thus localizes to the cytosol and especially to the nucleus; however, it is known that the attachment of peptides with membrane-targeting information leads to redistribution of YFP, especially and most obviously visible, to exclusion from the nucleus [43]. The diversity of membrane-targeting features, such as myristoylation, palmitoylation and/or polybasic regions, then define the cellular membranes at which the constructs preferentially accumulate [43].

In contrast with bacteria, CHO cells can perform S-acylation, a hydrophobic modification implicated in membrane binding, especially of intrinsically hydrophilic proteins. We therefore tested whether M2-CT–YFP is acylated despite the absence of the M2-TMD. CHO cells expressing M2-CT–YFP were labelled with [^{3}H]palmitate or [^{35}S]methionine/cysteine for 4 h, followed by immunoprecipitation with an anti-GFP antibody, SDS/PAGE and fluorography (Figure 4a). Figure 4(b) shows that M2-CT–YFP wt incorporated the radioactively labelled fatty acid. Since S-acylation is a post-translational event and (almost) always occurs on cellular membranes, M2-CT must have membrane-recognition features to become a substrate for palmitoylation. Disruption of the CRAC motifs (Y52S,Y57S) did not impede acylation, thus the tyrosine residues replaced in the CRAC motif

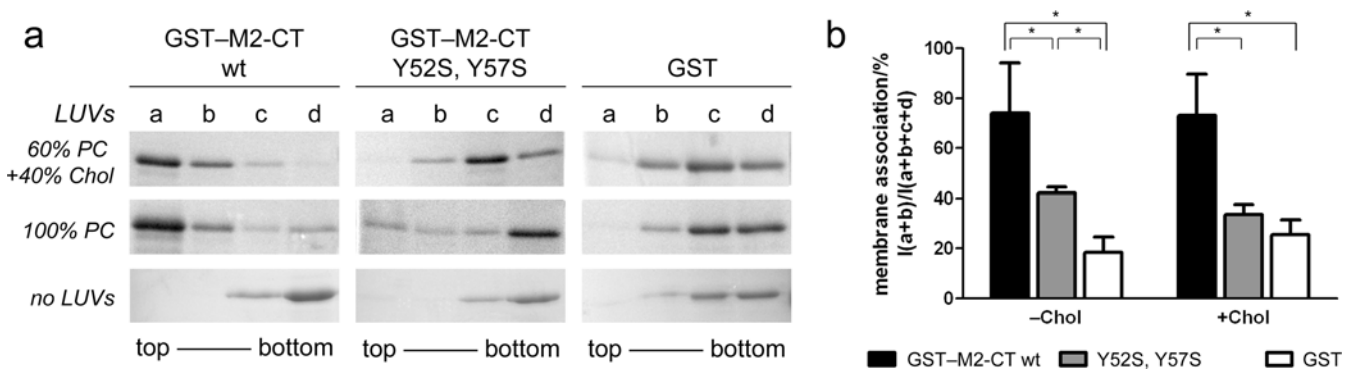

Figure 3 GST–M2-CT binds to LUVs

Purified GST–M2-CT wt, GST–M2-CT Y52S,Y57S or GST alone were incubated with LUVs composed of 60 % (mol/mol) PC (from egg) +40 % cholesterol (Chol), with 100 % PC LUVs, or without LUVs, and subjected to floatation analysis on a Nycodenz density gradient, which was divided into four equal fractions (a–d from top to bottom). (**a**) SDS/PAGE and Coomassie Blue staining of protein present in each fraction in one experiment. (**b**) Densitometric quantification of four independent experiments; protein in fractions a and b was defined as bound to LUVs. The percentage of membrane association $\pm$ S.E.M. [band intensity in fractions a + b/(a + b + c + d)] is shown. *Statistically significantly different according to two-tailed unpaired Student's t test ($P < 0.05$). Note the relatively large variability of membrane-associated protein between experiments, especially evident for GST–M2-CT wt. Since integral membrane proteins are present only in the uppermost fraction of the gradient in such an experiment [15], the distribution of M2-CT through many fractions indicates that membrane binding is not stable, but a transient and dynamic event.

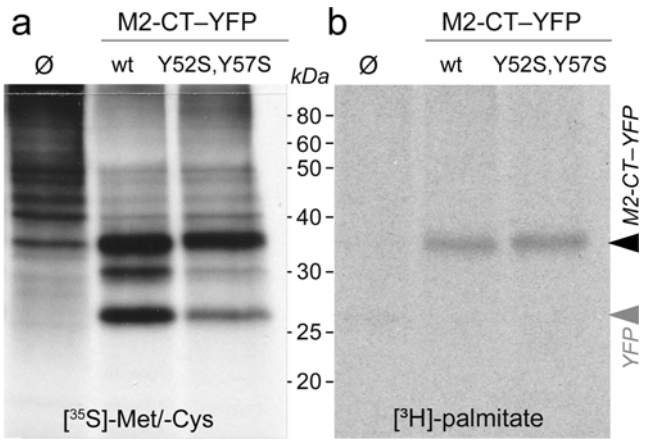

Figure 4 Acylation of M2-CT–YFP

CHO cells were transfected with M2-CT wt or M2-CT Y52S,Y57S as indicated or left untransfected (Ø), labelled with [^{35}S]methionine/cysteine (**a**) or [^{3}H]palmitate (**b**) for 4 h and subsequently lysed, followed by immunoprecipitation using anti-GFP antibodies, SDS/PAGE and fluorography. The arrows mark M2-CT–YFP (black) and YFP (grey), which is cleaved from M2-CT during sample preparation. The mobility of molecular mass markers is indicated in the middle.

mutant are not essential for initial membrane targeting and subsequent palmitoylation.

Next we examined the subcelluar localization of M2-CT–YFP by fluorescence microscopy. In transfected CHO cells M2-CT–YFP wt was (mostly) excluded from the nucleus and redistributed to intracellular compartments, especially to a perinuclear region (Figure 5a, top left-hand panel). This was identified as the Golgi apparatus by co-localization using marker antibodies against membrin, a Golgi-specific t-SNARE (target-soluble NEM-sensitive fusion protein-attachment protein receptor) (Figure 5c, bottom row). Some cells expressing M2-CT–YFP wt showed fluorescence distributed throughout the cytoplasm. Since it did not overlap with calreticulin, a marker for the ER (Figure 5c, top row), the signal is considered to be caused by soluble cytosolic protein.

Upon expression of mutants of M2-CT–YFP with a deleted acylation site (C50S), with replaced tyrosine residues (Y52S,Y57S) or with both lipid-binding sites deleted simultaneously (C50S,Y52S,Y57S), accumulation of fluorescence at the Golgi apparatus was less prominent and even localization to the nucleus was observed, especially for the mutants with disrupted CRAC motifs (Figure 5a, blue arrow). Since variation in the intracellular distribution of the fluorescence between individual cells occurred (see Figure 5a, especially evident for M2-CT with disrupted CRAC motifs), a (semi-)quantitative analysis of the micrographs was performed. Upon visual inspection of at least 125 cells, the fluorescence distribution in each cell was either considered as predominantly nuclear (see blue arrow in Figure 5a), perinuclear (Golgi, red arrow in Figure 5a), cytosolic (Figure 5c, top row) or, if no clear accumulation could be observed, uniform (cytosol plus nucleus, grey arrow in Figure 5a). This analysis demonstrated that M2-CT–YFP wt was localized to the Golgi apparatus (and, occasionally, to the plasma membrane) in 79 % of the cells investigated. In the remaining cases, the protein was present in the cytosol or uniformly distributed. The non-acylated mutant C50S was still found at the Golgi apparatus or the plasma membrane, but in only 52 % of the cells. Cytosolic accumulation of the protein was increased accordingly

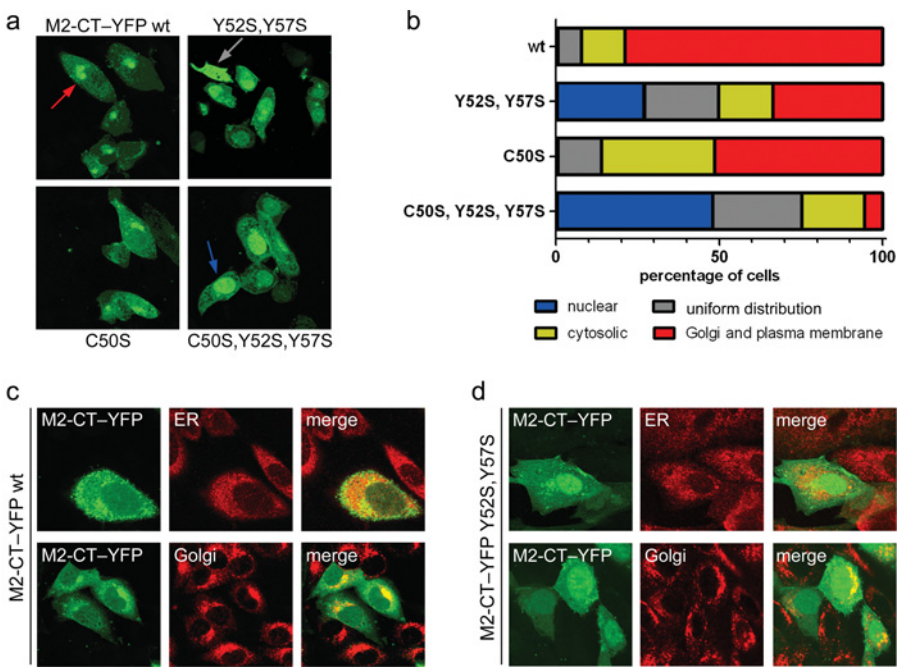

Figure 5 Subcellular localization of M2-CT–YFP wt and mutants

(**a**) Representative micrographs of CHO cells transfected with M2-CT–YFP wt and the indicated mutants thereof. Red arrow, cell with predominant signal at the Golgi apparatus (compare with **c** and **d**); blue arrow, nuclear localization; grey arrow, uniform distribution of fluorescence over the whole cell, including the nucleus. (**b**) Quantification of the subcellular localization of the indicated M2-CT–YFP constructs: at least 125 transfected cells were assessed for predominant localization of YFP fluorescence in the nucleus (blue), the cytosol (yellow) or at the Golgi and the plasma membrane (red, compare with **c** and **d**). Grey: uniform distribution. (**c** and **d**) Co-localization of M2-CT–YFP wt (**c**) or M2-CT–YFP Y52S,Y57S (**d**) with marker antibodies for the ER (anti-calreticulin, top row) or the Golgi (anti-membrin, bottom row) by indirect immunofluorescence. YFP is pseudocoloured green and secondary antibodies are pseudocoloured red; co-localization appears yellow in the corresponding merged image.

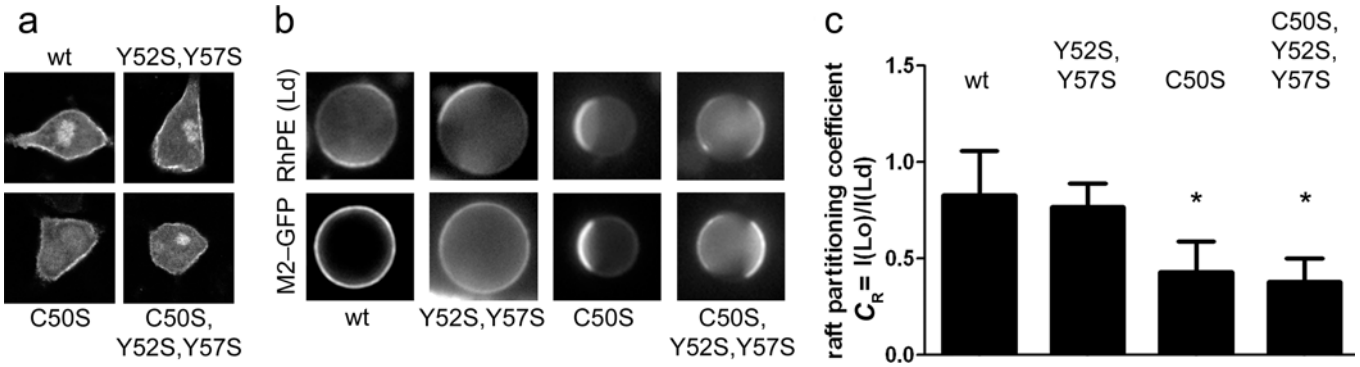

Figure 6 Partitioning of M2–GFP in the raft-like Lo phase of GPMVs

(**a**) Expression of M2–GFP wt and the indicated mutants thereof in RBL cells. (**b**) GPMVs were produced from RBL cells transfected with M2–GFP (wt or one of the indicated mutants), stained with RhPE as a marker for the Ld phase, cooled to 4 °C and visualized by epifluorescence microscopy. Representative images are shown. (**c**) Evaluation of raft partitioning: the GFP fluorescence intensity in the Lo and Ld phases of at least 12 GPMVs was determined and the 'raft partitioning coefficient' (C_R) was calculated as the GFP intensity in Lo/GFP intensity in Ld and displayed as the mean ± S.D. Values >1 indicate preference for Lo. *Statistically significant from wt according to one-tailed unpaired Student's *t* test ($P < 0.01$).

to 35 %. Thus palmitoylation of the amphiphilic helix stabilizes the intrinsic propensity of M2-CT to associate with the Golgi.

Replacing the CRAC motif tyrosine residues lowered the proportion of perinuclear localization of M2-CT–YFP further to 34 %. Figure 5(d) shows that this accumulation was not due to aggregation or precipitation of mutated protein since it co-localized with the Golgi marker. Likewise, the staining pattern considered as cytosolic did not overlap with the ER marker. Importantly, a strong nuclear signal was observed for M2-CT–YFP Y52S,Y57S in 27 % of the cells, indicative of the inability of this mutant to prevent nuclear accumulation of YFP. Lastly, expression of the mutant in which both the palmitoylation site and the CRAC motifs were disrupted (C50S,Y52S,Y57S) yielded only very few cells with Golgi accumulation of M2-CT (6 %). Rather, fluorescence was either observed throughout the cytoplasm (19 %) or uniformly distributed over the whole cell (27 %); predominant nuclear localization was seen in nearly half of the cells (48 %).

Taken together, these results indicate that M2-CT has the capacity to interact with cellular membranes, especially with the Golgi. Anchorage of M2-CT–YFP to the Golgi apparatus was most probably due to membrane association of the amphiphilic helix, since mutations in this region weakened Golgi localization with a pronounced contribution of both acylation and, even more strongly, the cholesterol-binding motifs, most effectively in combination. In the absence of the TMD, which functions as a signal-anchor domain in the authentic M2 protein [44], M2-CT is synthesized as a soluble protein on cytosolic ribosomes. The insertion of the tyrosine residues into the bilayer then probably mediates the attachment of the amphiphilic helix to the cytoplasmic leaflet of membranes, presumably intensified by the association with cholesterol, which is particularly abundant in the Golgi and the plasma membrane. Likewise, there might be a contribution to membrane attachment by the basic amino acids in the amphiphilic helix interacting with negatively charged phospholipids, such as phosphatidylserine, which is accumulated in the cytosolic leaflet of the Golgi and the plasma membrane. Palmitoylation, which is likely to occur at the Golgi apparatus [45,46], probably stabilizes membrane attachment of M2-CT–YFP. This allows the protein to enter the secretory pathway, but in contrast with other palmitoylated peripheral membrane proteins [45,47], targeting of M2-CT–YFP to the plasma membrane was observed only rarely. Since palmitoylation is potentially reversible [48], it can be assumed that the fatty acids are rapidly cleaved from the M2 construct. Since the stoichiometry of acylation cannot be inferred from metabolic-labelling experiments (Figure 4), it is possible that only a small subfraction of all M2-CT–YFP molecules carry a fatty acid under steady-state conditions, and therefore acylation contributes little to membrane binding of the protein. Surprisingly, mutations at the CRAC motif had a stronger effect on Golgi localization than removal of the palmitoylation site. Since palmitoylation at the adjacent cysteine residue was not impaired upon removal of the tyrosine residues (Figure 4), the hydrophobic residues directly affect membrane binding, i.e. by insertion into the lipid bilayer. In line with that, binding of the (non-acylated) purified M2-CT to liposomes was largely reduced by exchange of the bulky tyrosine residues with smaller serine residues (Figure 3).

M2 associates with both raft and non-raft domains in GPMVs

M2-CT–YFP was only infrequently targeted to the plasma membrane. Thus the M2 parts missing in the construct, especially the TMD, probably govern plasma membrane transport of M2. Accordingly, full-length M2 fused at its C-terminus to GFP was efficiently transported to the plasma membrane in transfected cells; mutating the palmitoylation site and/or the CRAC motifs did not inhibit plasma membrane transport (Figure 6a). Thus, in authentic M2, neither palmitoylation nor the CRAC motifs are required for transport of the protein to the plasma membrane, in line with previous studies by others [14,20].

We used these constructs to decipher the intrinsic propensity of M2 to associate with raft-like membrane phases. Using FLIM (fluorescence lifetime imaging microscopy)-FRET (fluorescence resonance energy transfer) we have previously shown that an identical construct (M2–YFP) does not associate with a double-acylated probe, a marker for small rafts present at the inner leaflet of bilayers [7]. However, the HA-containing viral budozone is larger and therefore regarded as a stabilized coalesced raft domain [4,5]. Coalesced raft phases can be produced in a cell-derived membrane model system, GPMVs. GPMVs are micron-scale blebs that can be formed from the plasma membrane of cells and thus contain the whole diversity of membrane lipids and proteins, but are detached from the cortical cytoskeleton. Upon cooling, large-scale phase separation into a ordered raft-like and a disordered non-raft phase [here also designated Lo ('liquid-ordered') and Ld ('liquid-disordered') respectively] is induced. [49]. In contrast with plasma membrane spheres [50],

GPMVs derived with NEM do not require cross-linking of compounds to reveal phase separation, and protein partitioning in these membranes thus resembles more closely that of the uninduced state of plasma membrane domains [35]. GPMVs were formed from the plasma membrane of RBL cells transiently expressing M2–GFP with a new method that preserves labile fatty-acid linkages [35] and were visualized by epifluorescence microscopy (Figure 6b). Staining of the non-raft phase with RhPE showed large-scale phase separation. However, M2–GFP wt was uniformly distributed over the whole GPMV membrane, implying no pronounced preference for either the Lo or Ld phase. This conclusion was substantiated further by calculating a 'raft partitioning coefficient' (C_R, ratio of the M2–GFP fluorescence intensities in Lo and Ld respectively) from at least 12 GPMVs, which yielded a mean value of 0.83 (Figure 6c). Using the same model system, it was shown that the transferrin receptor, a classical non-raft protein, is completely excluded from the raft domain, whereas typical raft markers, a GPI (glycosylphosphatidylinositol)-linked protein and LAT (linker for T-cell activation), are exclusively or predominantly present in the raft domain [35]. Thus, assuming that authentic M2 has the same distribution as M2–GFP, we conclude that M2 has an intermediate affinity for rafts in that model system. However, enrichment of M2–GFP at the boundary between the raft and non-raft-phase was not observed.

Do palmitoylation and cholesterol binding affect the phase partitioning behaviour of M2? The M2–GFP mutant with disrupted CRAC motifs (Y52S,Y57S) showed a comparable picture and a similar mean C_R value of 0.77. However, M2–GFP lacking the palmitoylation site (C50S) was clearly enriched in the non-raft Ld phase ($C_R = 0.43$). Both mutations in combination did not lead to a further decrease in raft-phase partitioning of the protein ($C_R = 0.38$). Thus the propensity of M2–GFP to associate with these raft phases depends on Cys^{50}, but not on the tyrosine residues in the CRAC motifs. This leads to the conclusion that cholesterol binding seems to be dispensable for the raft-association capability of M2, whereas palmitoylation is needed. Palmitoylation-dependent raft partitioning was also observed for a variety of other transmembrane proteins when GPMVs were prepared with the same method [35].

In summary, we have shown that (i) the CRAC motifs in M2-CT bind cholesterol, that (ii) the amphiphilic helix interacts with membranes, both *in vitro* and inside cells, and that (iii) M2 has the propensity to associate with large raft domains. The latter property is dependent on palmitoylation, but not on intact CRAC motifs, whereas both features are required for efficient membrane association of M2-CT.

In cholesterol-binding transmembrane proteins, such as the β_2-adenergic receptor [51] and the peripheral-type benzodiazepin receptor [38], the membrane-spanning helices build a cleft that accommodates cholesterol. Arginine or lysine residues located at the beginning of the transmembrane segment form electrostatic interactions with the hydroxy group of cholesterol, whereas aromatic residues, such as tryptophan or tyrosine, and long and hydrophobic residues (e.g. valine, isoleucine or leucine), both located in the hydrophobic region of the bilayer, interact with the planar sterol ring of cholesterol. These interactions lead to a parallel orientation of cholesterol and the transmembrane helices and thus align cholesterol perpendicular to the membrane bilayer. In contrast, binding of cholesterol to M2 does not require a transmembrane region, since the cytoplasmic tail alone was cross-linked to [^{3}H]photocholesterol (Figure 2). Thus the orientation of the cholesterol relative to the membrane bilayer might be different compared with cholesterol-binding transmembrane proteins. Nevertheless, tyrosine residues (or other aromatic amino acids, such as tryptophan) as part of the cholesterol-binding moiety have been shown to be essential for cholesterol binding in all hitherto analysed cholesterol-binding proteins [38,51]. It is conceivable that M2 sequesters cholesterol by means of its CRAC motifs and thereby lowers the local membrane cholesterol content. This could help in the ultimate budding step, the scission of nascent virus particles, which occurs at the phase boundary between the cholesterol-rich budozone and the (non-raft) bulk membrane. In accordance with that assumption is the observation that M2-mediated budding of vesicles into GUVs (giant unilamellar vesicles) occurs only if the cholesterol content in the GUV membrane is relatively low [29].

Not only are the tyrosine residues of the CRAC motifs involved in cholesterol binding, but they also contribute to membrane association of the amphiphilic helix. Golgi localization of M2-CT fused to YFP in transfected cells was substantially reduced when both tyrosine residues were deleted (Figure 5). This was probably not (only) due to an interaction with cholesterol, since association of purified non-acylated M2-CT with LUVs was not enhanced by cholesterol, but substantially reduced by replacing the tyrosine residues (Figure 3). Thus the amphiphilic helix of M2 has an intrinsic propensity to associate with membranes, which does not depend on acylation and cholesterol binding. The tyrosine residues, possibly in combination with surrounding basic residues, could interact with the interfacial region of membranes, whereas this interaction is greatly reduced when the tyrosine residues are replaced with serine residues [52].

Acylation is not strictly required for membrane binding, although a slight effect on Golgi localization of M2-CT–YFP was observed in transfected cells. However, palmitoylation is absolutely essential for M2–GFP to associate with the raft-like phase in GPMVs, whereas disruption of the CRAC motifs had no effect in that system (Figure 6). Since palmitoylation is a (at least potentially) reversible modification [48], addition and removal of fatty acids might regulate the lateral organization of M2 in the membrane. In order to mediate pinching-off of virus particles, it has been proposed that M2 must associate with the periphery of membrane rafts [22]. In virus-infected cells localization of M2 to the base of budding filaments (hence to the edge of the raft-like budozone) was seen [14,29]. However, we did not see accumulation of the M2 probe at the periphery of the coalesced raft phase. Therefore there are probably additional viral or cellular factors, for example the cytoskeleton [7], not accounted for in our GPMV model that lead to peripheral association of M2 with the budozone in virus-infected cells. Yet M2 has the intrinsic propensity to partially partition into a large more ordered membrane phase. Thus the key requirements of the proposed model for the function of M2 in particle scission, membrane association of the CT and (at least partial) raft-association, are in principle fulfilled.

AUTHOR CONTRIBUTION

Bastian Thaa performed the research, except for the results shown in Figure 6 which were carried out by Ilya Levental. Andreas Herrmann and Michael Veit were principal investigators and performed the research. Bastian Thaa and Michael Veit wrote the paper.

ACKNOWLEDGEMENTS

We thank Felix Wieland, Britta Brügger, F. Xabier Contreras and Timo Sachsenheimer (Biochemistry Centre, University of Heidelberg, Heidelberg, Germany) for providing [^{3}H]photocholesterol.

FUNDING

This work was supported by the German Research foundation (DFG) [grant numbers SFB 740 (TP C3), SPP 1175].

REFERENCES

1 Nayak, D. P., Balogun, R. A., Yamada, H., Zhou, Z. H. and Barman, S. (2009) Influenza virus morphogenesis and budding. Virus Res. **143**, 147–161
2 Rossman, J. S. and Lamb, R. A. (2011) Influenza virus assembly and budding. Virology **411**, 229–236
3 Lingwood, D. and Simons, K. (2010) Lipid rafts as a membrane-organizing principle. Science **327**, 46–50
4 Hess, S. T., Kumar, M., Verma, A., Farrington, J., Kenworthy, A. and Zimmerberg, J. (2005) Quantitative electron microscopy and fluorescence spectroscopy of the membrane distribution of influenza hemagglutinin. J. Cell Biol. **169**, 965–976
5 Leser, G. P. and Lamb, R. A. (2005) Influenza virus assembly and budding in raft-derived microdomains: a quantitative analysis of the surface distribution of HA, NA and M2 proteins. Virology **342**, 215–227
6 Zhang, J., Pekosz, A. and Lamb, R. A. (2000) Influenza virus assembly and lipid raft microdomains: a role for the cytoplasmic tails of the spike glycoproteins. J. Virol. **74**, 4634–4644
7 Thaa, B., Herrmann, A. and Veit, M. (2010) Intrinsic cytoskeleton-dependent clustering of influenza virus M2 protein with hemagglutinin assessed by FLIM-FRET. J. Virol. **84**, 12445–12449
8 Lamb, R. A., Zebedee, S. L. and Richardson, C. D. (1985) Influenza virus M2 protein is an integral membrane protein expressed on the infected-cell surface. Cell **40**, 627–633
9 Chen, B. J., Leser, G. P., Jackson, D. and Lamb, R. A. (2008) The influenza virus M2 protein cytoplasmic tail interacts with the M1 protein and influences virus assembly at the site of virus budding. J. Virol. **82**, 10059–10070
10 Iwatsuki-Horimoto, K., Horimoto, T., Noda, T., Kiso, M., Maeda, J., Watanabe, S., Muramoto, Y., Fujii, K. and Kawaoka, Y. (2006) The cytoplasmic tail of the influenza A virus M2 protein plays a role in viral assembly. J. Virol. **80**, 5233–5240
11 McCown, M. F. and Pekosz, A. (2005) The influenza A virus M2 cytoplasmic tail is required for infectious virus production and efficient genome packaging. J. Virol. **79**, 3595–3605
12 McCown, M. F. and Pekosz, A. (2006) Distinct domains of the influenza a virus M2 protein cytoplasmic tail mediate binding to the M1 protein and facilitate infectious virus production. J. Virol. **80**, 8178–8189
13 Zebedee, S. L. and Lamb, R. A. (1989) Growth restriction of influenza A virus by M2 protein antibody is genetically linked to the M1 protein. Proc. Natl. Acad. Sci. U.S.A. **86**, 1061–1065
14 Rossman, J. S., Jing, X., Leser, G. P., Balannik, V., Pinto, L. H. and Lamb, R. A. (2010) Influenza virus M2 ion channel protein is necessary for filamentous virion formation. J. Virol. **84**, 5078–5088
15 Thaa, B., Herrmann, A. and Veit, M. (2009) The polybasic region is not essential for membrane binding of the matrix protein M1 of influenza virus. Virology **383**, 150–155
16 Wang, D., Harmon, A., Jin, J., Francis, D. H., Christopher-Hennings, J., Nelson, E., Montelaro, R. C. and Li, F. (2010) The lack of an inherent membrane targeting signal is responsible for the failure of the matrix (M1) protein of influenza A virus to bud into virus-like particles. J. Virol. **84**, 4673–4681
17 Schnell, J. R. and Chou, J. J. (2008) Structure and mechanism of the M2 proton channel of influenza A virus. Nature **451**, 591–595
18 Sharma, M., Yi, M., Dong, H., Qin, H., Peterson, E., Busath, D. D., Zhou, H. X. and Cross, T. A. (2010) Insight into the mechanism of the influenza A proton channel from a structure in a lipid bilayer. Science **330**, 509–512
19 Nguyen, P. A., Soto, C. S., Polishchuk, A., Caputo, G. A., Tatko, C. D., Ma, C., Ohigashi, Y., Pinto, L. H., DeGrado, W. F. and Howard, K. P. (2008) pH-induced conformational change of the influenza M2 protein C-terminal domain. Biochemistry **47**, 9934–9936
20 Holsinger, L. J., Shaughnessy, M. A., Micko, A., Pinto, L. H. and Lamb, R. A. (1995) Analysis of the posttranslational modifications of the influenza virus M2 protein. J. Virol. **69**, 1219–1225
21 Veit, M., Klenk, H. D., Kendal, A. and Rott, R. (1991) The M2 protein of influenza A virus is acylated. J. Gen. Virol. **72**, 1461–1465
22 Schroeder, C., Heider, H., Moncke-Buchner, E. and Lin, T. I. (2005) The influenza virus ion channel and maturation cofactor M2 is a cholesterol-binding protein. Eur. Biophys. J. **34**, 52–66
23 Li, H. and Papadopoulos, V. (1998) Peripheral-type benzodiazepine receptor function in cholesterol transportIdentification of a putative cholesterol recognition/interaction amino acid sequence and consensus pattern. Endocrinology **139**, 4991–4997
24 Schroeder, C. (2010) Cholesterol-binding viral proteins in virus entry and morphogenesis. Subcell. Biochem. **51**, 77–108
25 Levental, I., Grzybek, M. and Simons, K. (2010) Greasing their way: lipid modifications determine protein association with membrane rafts. Biochemistry **49**, 6305–6316
26 Silvius, J. R. (2003) Role of cholesterol in lipid raft formation: lessons from lipid model systems. Biochim. Biophys. Acta **1610**, 174–183
27 Drin, G. and Antonny, B. (2010) Amphipathic helices and membrane curvature. FEBS Lett. **584**, 1840–1847
28 Zimmerberg, J. and Kozlov, M. M. (2006) How proteins produce cellular membrane curvature. Nat. Rev. Mol. Cell. Biol. **7**, 9–19
29 Rossman, J. S., Jing, X., Leser, G. P. and Lamb, R. A. (2010) Influenza virus M2 protein mediates ESCRT-independent membrane scission. Cell **142**, 902–913
30 Castrucci, M. R., Hughes, M., Calzoletti, L., Donatelli, I., Wells, K., Takada, A. and Kawaoka, Y. (1997) The cysteine residues of the M2 protein are not required for influenza A virus replication. Virology **238**, 128–134
31 Grantham, M. L., Wu, W. H., Lalime, E. N., Lorenzo, M. E., Klein, S. L. and Pekosz, A. (2009) Palmitoylation of the influenza A virus M2 protein is not required for virus replication in vitro but contributes to virus virulence. J. Virol. **83**, 8655–8661
32 Stewart, S. M., Wu, W. H., Lalime, E. N. and Pekosz, A. (2010) The cholesterol recognition/interaction amino acid consensus motif of the influenza A virus M2 protein is not required for virus replication but contributes to virulence. Virology **405**, 530–538
33 Veit, M., Ponimaskin, E. and Schmidt, M. F. (2008) Analysis of S-acylation of proteins. Methods Mol. Biol. **446**, 163–182
34 Thiele, C., Hannah, M. J., Fahrenholz, F. and Huttner, W. B. (2000) Cholesterol binds to synaptophysin and is required for biogenesis of synaptic vesicles. Nat. Cell Biol. **2**, 42–49
35 Levental, I., Lingwood, D., Grzybek, M., Coskun, U. and Simons, K. (2010) Palmitoylation regulates raft affinity for the majority of integral raft proteins. Proc. Natl. Acad. Sci. U.S.A. **107**, 22050–22054
36 Linder, M. E. and Deschenes, R. J. (2007) Palmitoylation: policing protein stability and traffic. Nat. Rev. Mol. Cell Biol. **8**, 74–84
37 Epand, R. M., Sayer, B. G. and Epand, R. F. (2005) Caveolin scaffolding region and cholesterol-rich domains in membranes. J. Mol. Biol. **345**, 339–350
38 Jamin, N., Neumann, J. M., Ostuni, M. A., Vu, T. K., Yao, Z. X., Murail, S., Robert, J. C., Giatzakis, C., Papadopoulos, V. and Lacapere, J. J. (2005) Characterization of the cholesterol recognition amino acid consensus sequence of the peripheral-type benzodiazepine receptor. Mol. Endocrinol. **19**, 588–594
39 Eisenberg, D., Weiss, R. M. and Terwilliger, T. C. (1982) The helical hydrophobic moment: a measure of the amphiphilicity of a helix. Nature **299**, 371–374
40 Eroglu, C., Brugger, B., Wieland, F. and Sinning, I. (2003) Glutamate-binding affinity of *Drosophila* metabotropic glutamate receptor is modulated by association with lipid rafts. Proc. Natl. Acad. Sci. U.S.A. **100**, 10219–10224
41 Li, H., Yao, Z., Degenhardt, B., Teper, G. and Papadopoulos, V. (2001) Cholesterol binding at the cholesterol recognition/ interaction amino acid consensus (CRAC) of the peripheral-type benzodiazepine receptor and inhibition of steroidogenesis by an HIV TAT-CRAC peptide. Proc. Natl. Acad. Sci. U.S.A. **98**, 1267–1272
42 Umashankar, M., Sanchez-San Martin, C., Liao, M., Reilly, B., Guo, A., Taylor, G. and Kielian, M. (2008) Differential cholesterol binding by class II fusion proteins determines membrane fusion properties. J. Virol. **82**, 9245–9253
43 McCabe, J. B. and Berthiaume, L. G. (1999) Functional roles for fatty acylated amino-terminal domains in subcellular localization. Mol. Biol. Cell **10**, 3771–3786
44 Hull, J. D., Gilmore, R. and Lamb, R. A. (1988) Integration of a small integral membrane protein, M2, of influenza virus into the endoplasmic reticulum: analysis of the internal signal-anchor domain of a protein with an ectoplasmic NH_2 terminus. J. Cell Biol. **106**, 1489–1498
45 Rocks, O., Gerauer, M., Vartak, N., Koch, S., Huang, Z. P., Pechlivanis, M., Kuhlmann, J., Brunsveld, L., Chandra, A., Ellinger, B. et al. (2010) The palmitoylation machinery is a spatially organizing system for peripheral membrane proteins. Cell **141**, 458–471
46 Veit, M. and Schmidt, M. F. (1993) Timing of palmitoylation of influenza virus hemagglutinin. FEBS Lett. **336**, 243–247
47 Salaun, C., Greaves, J. and Chamberlain, L. H. (2011) The intracellular dynamic of protein palmitoylation. J. Cell Biol. **191**, 1229–1238
48 Zeidman, R., Jackson, C. S. and Magee, A. I. (2009) Protein acyl thioesterases. Mol. Membr. Biol. **26**, 32–41
49 Baumgart, T., Hammond, A. T., Sengupta, P., Hess, S. T., Holowka, D. A., Baird, B. A. and Webb, W. W. (2007) Large-scale fluid/fluid phase separation of proteins and lipids in giant plasma membrane vesicles. Proc. Natl. Acad. Sci. U.S.A. **104**, 3165–3170
50 Lingwood, D., Ries, J., Schwille, P. and Simons, K. (2008) Plasma membranes are poised for activation of raft phase coalescence at physiological temperature. Proc. Natl. Acad. Sci. U.S.A. **105**, 10005–10010
51 Hanson, M. A., Cherezov, V., Griffith, M. T., Roth, C. B., Jaakola, V. P., Chien, E. Y., Velasquez, J., Kuhn, P. and Stevens, R. C. (2008) A specific cholesterol binding site is established by the 2.8 Å structure of the human β2-adrenergic receptor. Structure **16**, 897–905
52 Killian, J. A. and von Heijne, G. (2000) How proteins adapt to a membrane-water interface. Trends Biochem. Sci. **25**, 429–434

Received 19 April 2011/16 May 2011; accepted 19 May 2011
Published as BJ Immediate Publication 19 May 2011, doi:10.1042/BJ20110706